Cold Atom Interferometry

Mingsheng Zhan[1,2], Ke Li[1,2,3], Ping Wang[1,2,3], Lingbo Kong[1,2,3], Xiaorui Wang[1,2,3], Runbing Li[1,2,3], Xianhua Tu[1,2], Lingxiang He[1,2], Jin Wang[1,2], Baolong Lu[1,2]

[1]State Key Laboratory of Magnetic Resonance and Atomic and Molecular Physics, Wuhan Institute of Physics and Mathematics, Chinese Academy of Sciences, Wuhan 430071, P.R.China

[2] Center for Cold Atom Physics, Chinese Academy of Sciences, Wuhan 430071, P.R.China

[3] Graduate School, Chinese Academy of Sciences, Beijing 10080, P.R.China

E-mail: mszhan@wipm.ac.cn

Abstract In this article the recent experimental works on cold atoms carried out at Wuhan Institute of Physics and Mathematics (WIPM) are reported. These include the experimental realization of Bose-Einstein condensation (BEC), different type of cold atom interferometers, and bichromatic electromagnetically-induced transparency (EIT). We have realized Bose-Einstein condensates of ^{87}Rb dilute atomic gases. The apparatus consists of two horizontally mounted magneto-optic-traps (MOTs) and a QUIC magnetic trap. Nearly 3×10^8 atoms were trapped in the second MOT, and up to 1.2×10^8 atoms were adiabatically transferred to the QUIC trap. A pure condensate with about 1.1×10^5 atoms at about 30nK was achieved. We also demonstrated two type of cold atom interferometers, the Sagnac and Ramsey interference fringes were recorded with contrast of up to 37%.

1. Introduction

Cold atom physics and quantum information are two closely related fields that play important roles in recent interests in quantum computing, atomic frequency standards, high precision measurement, and understanding physics of degenerate Fermi gas.

For many years, we have carried out the study of laser cooling and trapping of neutral atoms, ion traps, quantum computation with nuclear magnetic resonance (NMR) of liquid molecules (see Fig.1 for the illustration). Our goal is to manipulate single particles (atoms, ions, or spins) for quantum computing.

Reported in this article are representative experimental progresses of the three aspects of coherence and interference studied in our group using laser cooled and trapped atoms. These include the realization of Bose-Einstein condensation (BEC) of Rb atoms, demonstration of cold atom interferometers, and bichromatic electromagnetically induced transparency (EIT) in cold atoms.
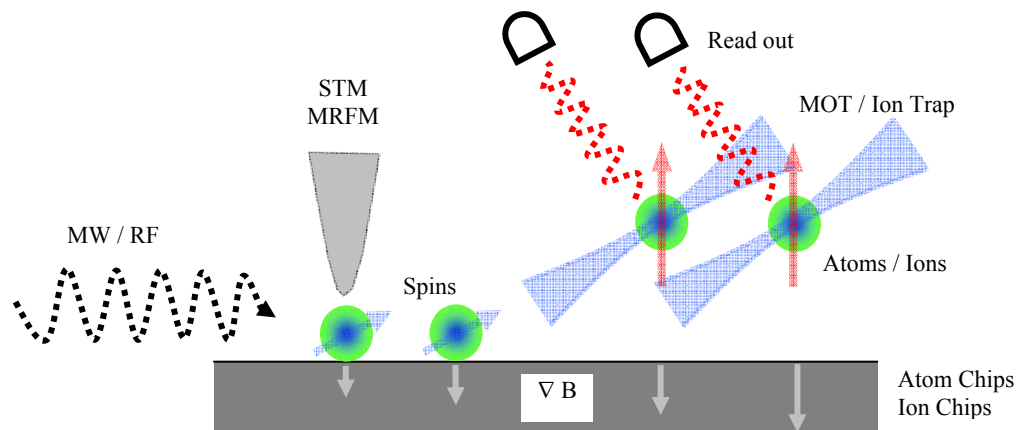
Fig.1 Scheme of manipulating single particles for quantum computation. Single ions, atoms or spins (atomic nuclei of molecules) are prepared, addressed, and coherently controlled by ion trap, magneto-optical trap (MOT), or magnetic resonance force microscopy (MRFM) with microwave (MW) or lasers.

2. ^{87}Rb BEC Experiment in WIPM

BEC [1] is a striking quantum mechanical phenomenon. In 1925, for the first time, Albert Einstein introduced the new notion of BEC based on Bose statistics [2,3], a method to derive the black-body spectrum. When a gas of bosons is cooled to so cold and dense that the de Broglie wavelength λ_{dB} is comparable to the interatomic separation, then atoms start to condense in the ground state. The concept of BEC is simple, but it had cost over 7 decades for scientist to realize it [4-6]. Since 1995, much interest has been focused on the research of the properties of the condensate [7-9], and there are several works that have also been done with the aim to explore the possible application of BEC [10,11]. Up to now, BEC has become a powerful tool in the research field of atomic optics, precision measurement and quantum physics.

In this paper, our apparatus and procedure to generate BEC in gas of ^{87}Rb are described. The apparatus consists of two horizontally mounted magneto-optic-traps (MOTs) and a QUIC magnetic trap [12,13]. The two MOTs were created in a rubidium vapor chamber and an ultra-high vacuum (UHV) chamber, respectively. The UHV MOT was loaded by continuous or pulsed atomic beams from the normal vapor cell MOT [14,15]. Nearly 3×10^8 atoms were trapped in the UHV MOT, and then the atomic cloud was further cooled to about 70 μK through polarization gradient cooling. After optically pumped to the state of $|F=2,m_F=2>$, up to 1.2×10^8 atoms were adiabatically transferred to the QUIC trap. Finally, the atomic cloud was evaporatively cooled by an external radio-frequency (RF) field swept from 25 MHz to 1.5 MHz over a period of 44s. At the end of the evaporative cooling, a pure condensate with about 1.1×10^5 atoms was achieved. Technique of time of flight (TOF) absorption imaging was used to study the properties of the BEC.

A schematic of the apparatus was shown in Fig.2. The whole apparatus was built on the optical table next to the laser system. The right part was also called high pressure(HP) MOT chamber, which was a rubidium vapor cell maintained at a pressure of about 5×10^{-8} Torr for routine experiment, and the pressure of the vapor of rubidium was adjustable by an all-metal valve (downside of the right part). The left part was called UHV MOT chamber, that was maintained at a pressure of about 2×10^{-11} Torr. Every MOT chamber was connected with a 6-way cross separately, and assembled in horizontal direction, that gives a 52.5cm horizontal distance between centers of the two MOTs. The 6-way cross was connected by a copper gasket, which was welded with a 150 mm long, 7mm diameter copper tube.
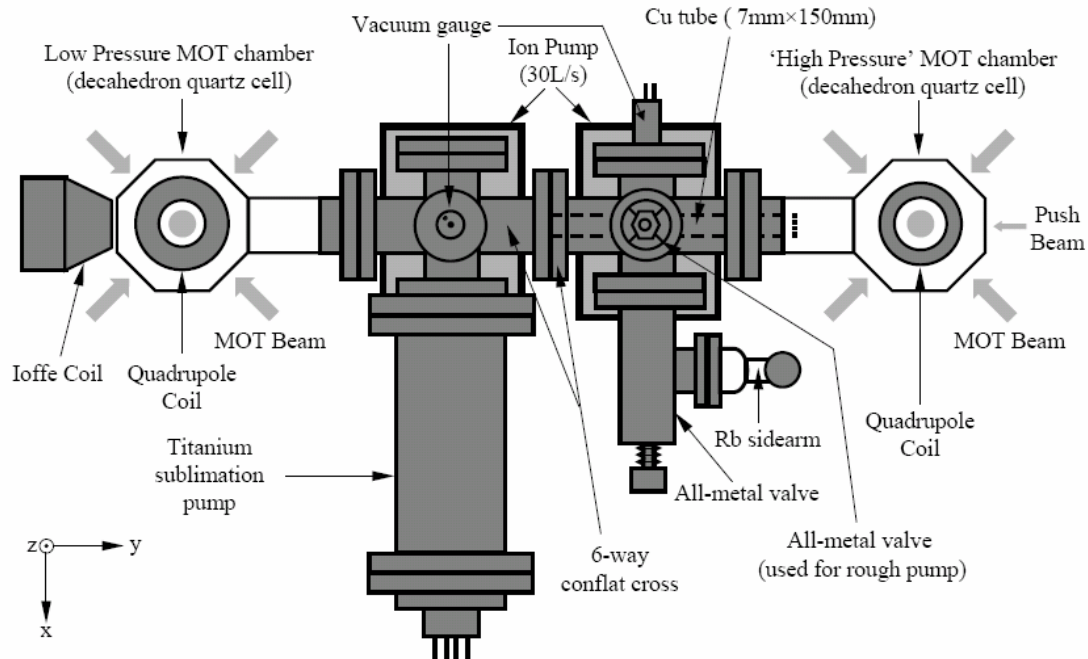
Fig. 2 Schematic of the BEC apparatus. Two 6-way conflat crosses were used to assemble the two MOT chamber in horizontal direction. An all metal valve (downside of the right 6-way cross) was used to control the vapor pressure of Rubidium. A sublimation pump (downside of the left 6-way cross) was used to raise the vacuum of the BEC chamber (low pressure MOT chamber). The whole vacuum system was built on top of two ion pumps. Two decahedron quartz cells were used, and the coils used to generate the fixed quadrupole and QUIC trap fields respectively are all located outside the chambers.

The copper tube presented a very small conductance for rubidium, so that robust differential pumping of the two chambers was maintained. The two connected 6-way crosses were mounted on top of two ion pumps (ULVAC GST-03L) that had the same speed of 30 L/s. A titanium sublimation pump was connected to one sidearm of the 6-way cross on the left part, aiming to improve the vacuum level of the UHV MOT chamber. The 6-way cross on the right part was connected with an all metal valves on top of it that facilitated rough pumping to pressure below 10^{-7} Torr before the ion pump and sublimation pump could be activated.
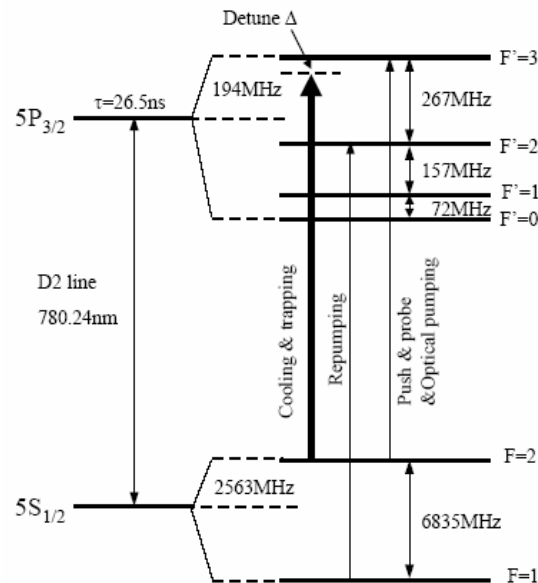
Fig.3 Relevant energy levels and optical transitions encountered in the experiment of generating [87]Rb BEC.

Fig.3 depicts the relevant energy levels and optical transitions involved in the experiment of generating [87]Rb BEC. The work of cooling and trapping of rubidium was due to the so called 'trapping laser', which was frequency controlled by a double-pass acoustic-optical modulator (AOM) configuration. Trapping laser with controllable red detuning of 15 to 50 MHz from the resonance transition [87]Rb, $5S_{1/2}$, F=2→$5P_{3/2}$, F=3 was essential for the implementation of the laser cooling. An additional diode laser was used as the so called 'repumping laser', that was tuned to [87]Rb, $5S_{1/2}$, F=1→$5P_{3/2}$, F=2 transition using the saturation spectroscopy technique. The total 600 mW laser power produced by the Ti:sapphire laser was divided into three parts. Three sets of double-pass AOM configurations were used to control the frequencies of these laser beams respectively, and this gave the convenience for separately controlling the trapping laser beams of the double MOT, as well as the push beam, optical pumping beam and probe beam.

Fibers were used to transport the two trapping laser beams to reach the optics surrounding the two MOTs. Trapping laser beams of each MOT overlapped with the corresponding repumping laser beams, that was the general configuration of the MOT beams. The double MOTs had the same MOT laser-beam geometry, which consisted of three pairs of mutually counter-propagating beams. One of the beam axes was oriented along the vertical z axis and the other two beam axes were oriented along the diagonals in the x-y plane. All laser beams, except for the repumping beams, were derived from the Ti:sapphire laser that was stabilized using polarization spectra signal [16], and with a frequency stability of better than 2 MHz. The MOT beams were expanded to a diameter of 23 mm for the HP MOT and the UHV MOT, respectively.

The atoms were first laser cooled and accumulated in the HP MOT, then a pushing beam gave the atoms an initial momentum and the atoms flew down the copper tube to the UHV MOT. The push laser beam was aligned to pass through the center of the HP MOT along the copper tube, and about 3 mm above the center of the UHV MOT. In fact, the push beam may disturb the UHV MOT, leading to the decrease of atomic numbers. A lens with 100 cm focal length was used to focus the push beam that caused a smaller spread in atomic transverse velocity, and the interaction between the UHV MOT and the push beam was strongly reduced. In order to further reduce this interaction and load more atoms into UHV MOT, pulsed push light (I_{push}=36mW/cm^2, Δ = 0 MHz) was used. The present transfer sequence for a maximum number of atoms in UHV MOT was: (i) Turn the HP MOT beams on, and

load the MOT for 100 ms. (ii) Turn off the HP MOT laser beams, and turn on the push beam for 0.8 ms. (iii) Turn off the push beam and wait an additional 4.2 ms. So the pushed atoms have enough time to leave the capture region of the HP MOT for the UHV MOT. This sequence was repeated for up to 60s until the number of atoms in UHV MOT reached a steady value.

High flux of atoms from HP MOT was needed for the sake of rapid generation of BEC. The capture rate of HP MOT is [17]

$$\frac{dN}{dt} = \frac{N_s}{\tau} e^{-t/\tau} \qquad\qquad (1)$$

where N is the number of atoms accumulated in the HP MOT, N_s is the steady-state atom number in the same MOT, and τ is the 1/e time of the accumulation rate in the MOT. When the accumulation time t=τ, the rate that atoms accumulated in the HP MOT decreased to 1/e of N_s/τ. This implies that only continuous push beam can produce a maximum flux from the HP MOT. But the long interaction time between the HP MOT and the push beam prevented the UHV MOT from reaching its maximum. Thus the total intensity (I_{trap}) of the UHV MOT trapping laser must be much higher than that of the push beam. Our first BEC was realized by using continuous atomic beam with $I_{trap}>20\ I_{push}$. And now, pulsed atom beam was used in our working BEC apparatus for the sake of (i) reducing the requirement of high power; (ii) more atoms needed to be loaded into the UHV MOT, and consequently, more atoms transferred to the QUIC trap.
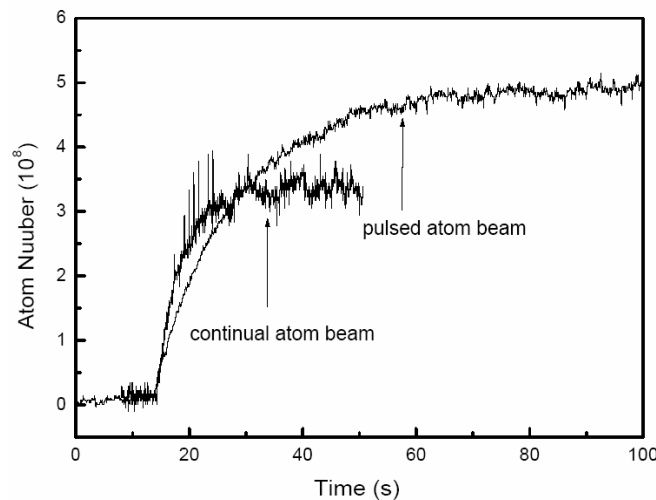

Fig.4 Loading curve of the UHV MOT. Atom number was determined through measuring the fluorescence light power of atoms in the MOT. The fill curve of ^{87}Rb atoms in UHV MOT can be fitted by an exponential function. When continuous atomic beam was used, the maximum atom number in UHV MOT could reach to 3×10^8, the fill time constant was 4.2s. When pulsed atomic beam was used, the maximum atom number in UHV MOT was increased to 5×10^8, and longer fill time constant, 15.1s, was needed.

Fig.4 shows the loading curve of the UHV MOT under different loading conditions. In the loading experiment using continuous atom beam on the double MOT, trap beams with a diameter of 1.6 cm were used for the UHV MOT, and no fiber was used to filter the trap laser beam, that raised the total laser intensity by a factor of 3.8. The total loading time usually was 30s when using the continuous atomic beam. But this caused many difficulties in the operation of the system.

Right after the UHV MOT was fully loaded, the so-called compressed MOT (CMOT) was performed: (i) Shut off the push beam to finish loading process. (ii) Further detune the cooling laser of UHV MOT from -15MHz to -24MHz to reduce heating. (iii) Ramp up the axial gradient of the UHV MOT quadrupole magnetic field from 10 G/cm to 20 G/cm in 20ms.

After the CMOT process, the atom density in UHV MOT was increased several times as a rule, but the temperature still high. The polarization gradient cooling (PGC) was used to further cool the atoms beyond the Doppler limit [18]. For the sensitivity to magnetic field, an effective PGC process requires the residual field to be less than 100 mG [19]. For this reason the MOT quadrupole magnetic field must be shut off, and three orthogonal pairs of rectangular Helmholtz coils, that centered around the UHV MOT cell, were used to cancel the ambient magnetic field to be less than 50 mG. PGC was carried out right after the CMOT process: (i) Shut off the current to the UHV MOT quadrupole coils. (ii) Further detune cooling laser from –24 MHz to –58 MHz and maintain 4 ms. Temperature of atom cloud could be reduced to less than 70 μK after PGC.

Optical pumping is a process whereby one increases the number of magnetically trappable atoms. For magnetic trapping of rubidium atoms, we need to enhance the population of weak field seeking ^{87}Rb $|F=2, m_F=2\rangle$ states. Right after PGC process, trapping laser beam was shut off by the AOM that was used to modulate the frequency and power of UHV MOT trapping beams. And additional mechanical shutter was used to block the residual trapping laser beam. A σ^+ circularly polarized laser beam was used to pump on the $F=2 \rightarrow F=3$ resonance transition. A small referential magnetic field of 1.0 G was applied using the pair of coils that along direction of the pump laser beam's axis of propagation. The atoms were optically pumped for 1.0 ms with a collimated optical pumping laser beam of $I = 0.08$mW/cm^2.

The QUIC trap consists of two identical quadrupole coils with 202 windings which are also used to create UHV MOT's quadrupole magnetic field, and one Ioffe coil with 338 windings. Fig.5 is a schematic of the QUIC trap, and all dimensions were lined out in unit of mm. In the QUIC configuration the trap had a radial gradient of 190 G/cm and the axial curvature was 168 G/cm^2, with a current of 21.5A running through all three coils. The bias field of 1.5 G resulted in trapping frequencies of $2\pi\times198$ Hz in the radial and $2\pi\times16.5$ Hz in the axial direction, for rubidium atoms in the $5S_{1/2}$ $|F = 2, m_F = 2\rangle$ state.
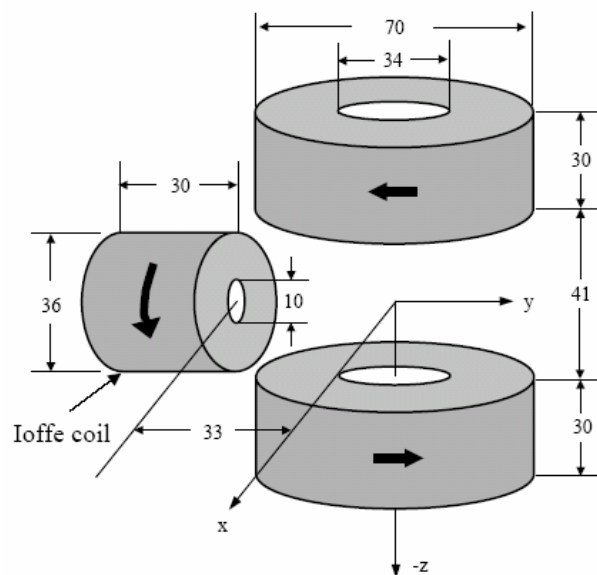

Fig.5   Schematic of the QUIC trap. The QUIC trap consists of three cylindrical coils, and all dimensions in the schematic are in unit of mm. The bold face arrows indicate directions of current in each coil.

After optical pumping the current in quadrupole coils was increased from 0 to 12 A, and an additional mechanical shutter was used to block the residual light from the fiber that carrying the pumping laser. Then the referential field was turned off, and atom cloud was compressed adiabatically by increasing current in the quadrupole coils from 12 to 21.5 A in 2s. Current in the Ioffe coil was subsequently increased from 0 to 21.5 A in 2.2s, such that the QUIC trap was formed. The minimum of the quadrupole trap and the QUIC trap were not the same, they had a distance of 10.6 mm along y axis. During the transferring process, atom cloud followed the initial shifting (with small deformation) of minimum of the trapping potential. Before the QUIC configuration was reached, the second minimum (of the second quadrupole potential) formed near the Ioffe coil in the –y direction, and atom cloud followed a large deformation and spilled out over into the second quadrupole magnetic well. As current in the Ioffe coil was further increased, minimums of the double well moved toward each other until they met and formed harmonic potential of the QUIC trap.

Up to 1.2×10^8 atoms were transferred into the QUIC trap with the temperature up to 870 μK. This gave the magnetically trapped atom cloud an initial mean elastic collision rate γ_{el} = 15Hz. Number of the magnetically trapped atoms decays as $N(t)=N(0)e^{-t/\tau}$, where τ is the 1/e lifetime of the atom cloud in the QUIC trap. Atom number measured after a variable holding time in the QUIC trap gave the lifetime τ = 155s with the background pressure lower than 2×10^{-11} Torr in the UHV MOT chamber. The condition for runaway evaporative cooling was fulfilled by $\gamma_{el}\tau >>150$.

The key technique named evaporative cooling was used at the finial cooling stage to increase the phase space density (PSD) of the atom cloud. The two-turn RF coil with a diameter of 46 mm was constructed from 1 mm copper wire. The RF coil was placed 37 mm away from the center of the QUIC trap, and oriented to radiate RF photons propagating along –x axis. Evaporative cooling of the atoms was performed sweeping RF frequency from 25MHz to around 1.5MHz over a period of 44s. Details of the sweeping trajectory consisted of four stages. In each of the four evaporation stages, the time-dependent RF frequency followed the form [19]

$$v(t) = v_{base} + (v_{start} - v_{base})e^{-t/\tau_{RF}}, \quad 0 < t < \tau_{RF} \ln\left(\frac{v_{start} - v_{base}}{v_{stop} - v_{base}}\right) \tag{2}$$

Each stage of evaporative cooling was optimized by observing increasing of the max optical density deduced from absorption imaging as the evaporation parameters v_{start}, v_{stop}, v_{base} and τ_{RF} were varied. A Standford Research System (SRS) DS345 30MHz synthesized function generator was used to generate the RF signal, then amplified by a mini-circuits RF amplifier (TIA-1000-1R8-2). In our routinely evaporative cooling experiments, about 1 watt of RF power was used to realize BEC. The SRS DS345 was computer controlled using a GPIB card, such that arbitrary frequency of RF signal with a 30ms update interval was realized.

Absorption imaging was used to probe cold atoms. Light passes through atomic cloud and results in reducing of intensity in its propagating direction. This is given by the Beer's law

$$I = I_0 e^{-OD} \tag{3}$$

where I_0 and I are the intensities incident and emerging from the atom cloud respectively. In experiment, the optical pumping beam was also used as probe beam with a different light intensity of 0.16mW/cm². A charge coupled device (CCD) was used to record intensity of the probe beam passing through the imaging system. Our imaging system was a 4f imaging system with a 70mm focus lens that gave a magnification of 1.

At the end of evaporative cooling, current running through the QUIC coils was shut off in less than 1 ms to release the cloud from the magnetic trap. After a time of ballistic expansion, a typically 100 μs

σ^+ circularly polarized laser pulse, that tuned to the F=2→F=3 resonant transition of the D2 line, was used to shine on the cloud. Absorption of imaging light was imaged onto the CCD camera by the imaging system. We must take the other two images (one with imaging light only, one without imaging light and atoms), so that quantitative information about the atom cloud can be obtained. The three images were named by $I_{atom}(y,z)$, $I_{light}(y,z)$, $I_{dark}(y,z)$. The average optical density (OD) over each pixel of CCD (with a resolution of 6.8μm × 6.8μm) of the atomic cloud was given by

$$OD(y,z) = \ln\left(\frac{I_{light}(y,z) - I_{dark}(y,z)}{I_{atom}(y,z) - I_{dark}(y,z)}\right) \qquad (4)$$

The total number of atoms N was calculated by

$$N = \frac{1}{\sigma_0} \sum_y \sum_z OD(y,z) \qquad (5)$$

where σ_0 is the resonant scattering cross-section for circularly polarized laser light. The procedure currently used to derive total atom number, temperature, and density of the atomic cloud from the absorption images was a MATLAB program. This program was designed to execute three different fitting routines depending on the degeneracy of the cloud. For clouds outclassing the condensation temperature, Gaussian fit was always used to fit the OD matrix. Clouds for a bimodal distribution were fitted with a combined function of a Gaussian distribution function and a Thomas-Fermi distribution function. For pure condensate, only Thomas-Fermi distribution function was used. Absorption imaging was used to imaging atomic cloud both in MOT and QUIC trap, and information about the atomic cloud was all deduced by the MATLAB program.

Transition from thermal cloud with atoms in normal phase to BEC phase was observed by absorption imaging. Fig.6 depicted onset of BEC. The total ramping time of RF frequency was fixed (in order to hold constant heating of the QUIC coils), column density distribution in atomic cloud varied with the truncation frequency. For truncation frequency above 1460 KHz, only a normal density distribution existed (Fig.6 left). At 1460 KHz, bi-model distribution to the cloud appeared (Fig.6 middle) with total 4.5×10^5 atoms at a temperature of 233 nK. Further evaporative cooling resulted in a pure condensate containing 1.1×10^5 atoms. Transition from normal cloud to BEC gave the 300nK critical temperature that a condensate formed in our experiment.
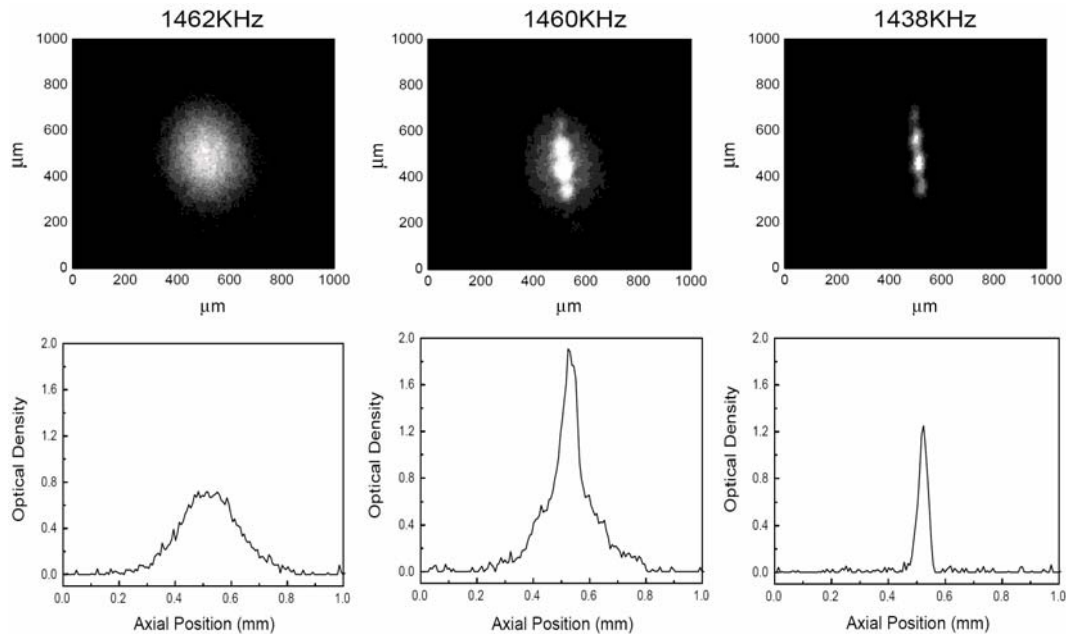
Fig.6 Onset of BEC. The top three absorption images were taken after 20ms free expansion of the atom cloud. The figures represent: (left) thermal atoms with $T>T_c$, (middle) bi-model distribution of atoms (partial atoms condensed) with $T\sim T_c$, (right) almost pure condensate with 1.1×10^5 atoms. $T_c \approx 300$nK.

Multi-component caused by Majorana transitions was also found in Fig.6. Long time of free expansion of the BEC was operated to observe the separated peaks. Evolution of axial to radial aspect ratios for the condensate was also studied.

The QUIC trap with three coils had a relative simple configuration, and its stability of magnetic trapping field facilitated evaporative cooling. A somewhat large decahedron quartz cells for the UHV MOT in our apparatus resulted in a large Ioffe coil and heating of the Ioffe coil could not be avoided, that gave the up-shifting of bias magnetic field of our QUIC trap. During the 44s evaporative cooling, bias magnetic field was up-shifted to 2.093G (derived from evaporative cooling), and the radial trapping frequency was reduced to about $2\pi\times171$Hz. Additional 6 minutes was needed to wait for the Ioffe coil to completely cool to room temperature. When the total evaporative cooling time was hold as a constant, the bias magnetic field could be repeated with very small long-term drifting. Quartz cells used for double-MOT that was assembled in horizontal direction gave the apparatus excellent optical access and a compact nature. Further experiments such as BEC in optical lattice [20] and interference of two BEC [21] can be operated with this apparatus.

3. Demonstration of a Sagnac-Type Cold Atom Interferometer

Since the first demonstration in 1991, atom interferometer [22-24] has proven the importance in testing foundations of quantum mechanics, manipulating the wave functions coherently and in metrology of time and frequency, and other applications as precise inertial sensors such as gyroscopes and accelerometers. With the development of laser cooling and trapping techniques, early atom interferometers that use thermal atomic beams [25-26] desire to choose laser cooled atoms as the more ideal atom source which has the merit of lower velocity and temperature. Examples of cold atom interferometers include exact measurement of the Newtonian constant of gravitation *G* and absolute-gravity-gradient [27-30], accurate measurement of photon recoil [31], and precise determination of the fine-structure constant α [32]. More recently, even ultracold Bose-Einstein condensed atoms have also been used by Torii *et al.* in constructing a Mach-Zehnder interferometer and in studying the optical

Bragg diffraction [33]. The experiment for a cold atom interferometer was initially to use the atom fountain, in which the atomic wave packets interfere along the gravity direction. The Sagnac-type atom interferometer used to sense rotation was achieved in a transversely launched cold atom cloud, which was reported only recently [34].

Sensitivity to rotation due to Sagnac effect can be enhanced greatly by using atoms instead of photons. We can understand this from the expression of phase shift caused by Sagnac effect

$$\Delta\phi = \frac{4\pi\ \Omega A}{\lambda_{dB}V} \qquad (6)$$

where Ω is the angular velocity of rotation, A is the area enclosed by interference loop, and V is the particle velocity which is much slower than the light speed in vacuum. λ_{dB} denotes the de Broglie wavelength of a massive particle which is greatly shorter than light wavelength. To sense a rotation, atom beam is coherently manipulated by Raman lasers, and an enclosed area is formed by two indistinguishable paths. In this case, k-vector of the Raman lasers is perpendicular to atomic motion, and the two laser beams are chosen in co-propagating (Doppler insensitive) or counter-propagating (Doppler sensitive) configurations. In co-propagating configuration, atom acquires recoil kick of the photons by amount of $\hbar(\mathbf{k}_1 - \mathbf{k}_2) = \hbar(|\mathbf{k}_1| - |\mathbf{k}_2|)$, which is quite small as compared with $\hbar(\mathbf{k}_1 - \mathbf{k}_2) = \hbar(|\mathbf{k}_1| + |\mathbf{k}_2|)$ in the counter-propagating case.

The Raman pulse sequence $\pi/2$-π-$\pi/2$ is normally used to shape an interference loop. The first $\pi/2$ pulse separates the atom into two paths, and puts atom into a superposition internal state simultaneously. The following π pulse reflects the atom, and the internal states are swapped. The last $\pi/2$ pulse recombines the atom wave packet. The relative phases $\varphi(t_1)$, $\varphi(t_2)$, and $\varphi(t_3)$ of the three pairs of Raman pulses are related to the population in the following way

$$P_{e,g} = \frac{1}{2}[1 \pm \cos(\varphi(t_1) - 2\varphi(t_2) + \varphi(t_3))] = \frac{1}{2}[1 \pm \cos(\Delta\Phi)] \qquad (7)$$

If one changes $\varphi(t_3)$ while keeping $\varphi(t_1)$ and $\varphi(t_2)$ unchanged, the population will be changed with $\varphi(t_3)$ in the form of a cosine function. The Sagnac phase shift for rotation can be accurately transferred to atom population in a certain atom state.

The schematic diagram of our experimental setup is shown in Fig.7. Atoms were firstly cooled and about 10^8 atoms were trapped in the MOT [15], the cold atom cloud was pushed transversely by a duration of 700 μs resonant light pulse [35] to the interference chamber at a speed of 24 m/s. Three pairs of counter-propagating trapping beams were (1,1,1) configuration. Each pair was $\sigma^+ - \sigma^-$ polarized with equal intensity. The trapping beam was split into six equal-intensity beams by combining half-wave plates (HWPs) and polarization-beam-splitters (PBSs). A single-mode polarization-maintenance optical fibre was used to transmit and to spatially filter all the laser beams from the optical desk to the vacuum chambers. The cold atomic flux spent around 30ms to fly across the Raman laser pairs and to the detection region.
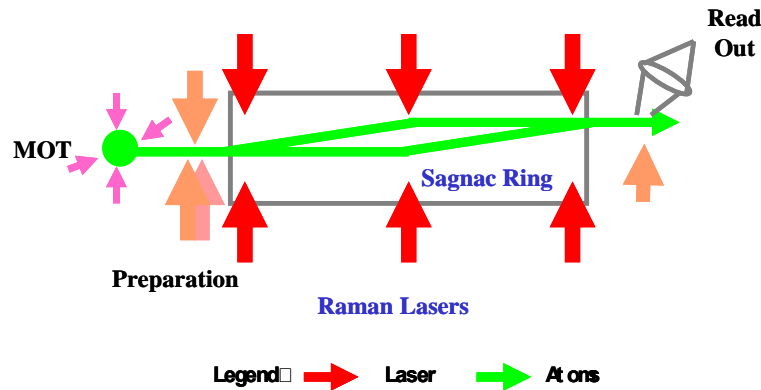
Fig. 7 Experimental arrangement of the transverse cold atom Sagnac-type interferometer. Cold Rb atoms are prepared in the magneto-optical trap (MOT). Push laser pulse loads the atom cloud to the interference region consisting of Raman laser pulse sequence $\pi/2$-π-$\pi/2$. Laser-induced fluorescence (LIF) signal is recorded in the read out region.

An optical pumping light (shown in Fig. 8, or preparation light in Fig. 7) resonant with the $5S_{1/2}$, $F=3\leftrightarrow5P_{3/2}$, $F' =3$ transition was applied to pump all atoms to $F=2$. Magnetic insensitive Zeeman sublevel, $m_F=0$, was chosen for investigation of atomic interference. Other Zeeman sublevels were shifted out of resonance of Raman laser pair. Following state preparation, atoms interacted with the $\pi/2$-π-$\pi/2$ Raman pulse sequence. When atoms are driven by the first $\pi/2$ Doppler insensitive Raman pulse, they coherently evolve into superposition of two ground states, $F=2$, $m_F =0$ and $F=3$, $m_F =0$. After 4.8 ms free flight, atoms travel through the π pulse and exchange their states. Then the atoms travel through the second $\pi/2$ pulse, and the wave packets interfere with each other. At the end of the chamber a photo multiplier tube (PMT) was used to detect the fluorescence induced by a resonant detection leaser. The fluorescence induced by the detection laser from the state $F=3$, $m_F =0$ was recorded to analyse the state population.
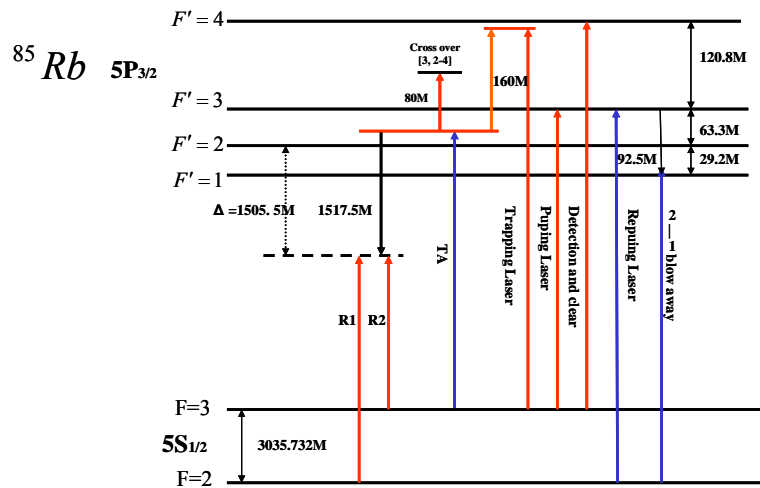

Fig. 8 ^{85}Rb atomic energy levels and laser frequencies. The frequency of main laser (TA) is locked to the $F=3\rightarrow F'=$ (2, 4 crossover) resonance peak. Raman transition is realized between the ground states of $5^2S_{1/2}$ ($F=2$) and $5^2S_{1/2}$ ($F=3$) by two Raman beams R1 and R2.

The theory of atom interferometer is based on a three-level system underlying the two-photon stimulated Raman transition [36]. As shown in Fig. 8, laser fields ω_1(R1) and ω_2(R2) can couple states $|g\rangle \equiv |F=2, m_F=0\rangle$ and $|e\rangle \equiv |F=3, m_F=0\rangle$ by an intermediate state $|i>$. The atom first absorbs one photon with frequency ω_1, and then is stimulated to emit one photon with frequency ω_2. The large detuning Δ of the laser frequencies from the excited state $|i>$ greatly inhibits the spontaneous decay, and the system can be treated effectively as a two-level system.

The Hamiltonian for the three-level system reads

$$H = \hbar\omega_g |g\rangle\langle g| + \hbar\omega_i |i\rangle\langle i| + \hbar\omega_e |e\rangle\langle e| - \vec{d}\cdot\vec{E} \qquad (8)$$

The field in which atoms suffered can be described as a superposition of two individual laser fields,

$$\vec{E} = \vec{E}_1 \cos(\vec{k}_1\cdot\vec{x} - \omega_1 t + \phi_1) + \vec{E}_2 \cos(\vec{k}_2\cdot\vec{x} - \omega_2 t + \phi_2) \qquad (9)$$

The effective Rabi frequency Ω_{eff} of coupling the two ground states is expressed as

$$\Omega_{eff} = \frac{\Omega_1\Omega_2}{2\Delta} \qquad (10)$$

where Ω_1 and Ω_2 are the single-photon Rabi frequencies, respectively.

Two-photon Raman [37-38] pulse drives Rabi oscillations between two hyperfine levels of the ground electronic state of Rb atoms. As illustrated in Fig. 7, three Raman laser pairs work in a continuous way. The pulse area defined as $\pi/2$ or π is determined by changing the laser intensity for the given transit time of moving atom through the Raman beam. A Raman laser pair was generated by the ± 1 order output from an acoustic-optical modulator (AOM, Brimrose GPF-1500-200-.780) with carry frequency of 1.5 GHz supplied by an analog signal generator (HP/Agilent E8257C PSG), which was externally referenced to a hydrogen atomic clock (Shanghai Astronomical Observatory SOHM-III). The main laser (TOPTICA TA100) was locked to the crossover peak of $F=3\rightarrow F'=2$ and $F=3\rightarrow F'=4$ (see Fig. 8). The Raman lasers R1 and R2 were phase-correlated with each other, and they also had a stable frequency difference of 3.0 GHz, which was exactly equal to the energy level separation of the two ground states of ^{85}Rb. Meanwhile R1 and R2 were commonly detuned about 1.5 GHz from the $5P_{3/2}$, $F'=3$ hyperfine level.

The two Raman beams were overlapped with orthogonal linear polarizations by a PBS cube and then coupled into the fibre. Because any change in the relative paths of the two Raman beams due to vibrations of the beam steering optics will be seen as spurious interference phase shift, vibration isolation is necessary. Co-propagating beams in the optic fibre also minimized the potential phase shift of the Raman light. The fibre filtered Gaussian beam was collimated, its diameter ($1/e^2$ intensity contour) was about 1 cm, and it was divided into three parts as $\pi/2$-π-$\pi/2$ pulse pairs. An electro-optical modulator (EOM, New Focus 4002) was used as a phase modulator to change the relative phase of the final $\pi/2$ pulse, $\varphi(t_3)$. The intensity ratio of Raman beam-pair R1:R2 can be optimized to minimize unwanted ac Stark shifts [37].

We have observed Rabi oscillations when varying total Raman-pair intensity while keeping the intensity ratio constant (1:5.3). Raman beams were in co-propagating configuration, and the frequencies were detuned with $\Delta=1.5$ GHz away from the resonances. The experimental result is shown by the dots in Fig. 9, and the fitting result is illustrated by the solid line. The dots show clearly the dependence of population of the $F=3$ state on intensity of Raman beams, it is a gradually attenuated sine wave, and the maxima appear at 2.1 mW and 4.7 mW.
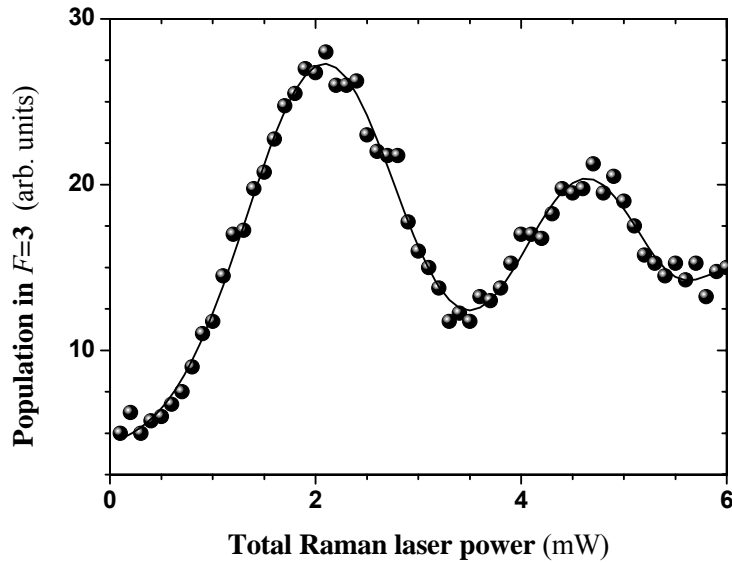
Fig. 9 Rabi oscillations for co-propagating Raman beams with detuning Δ=1.5 GHz. Dotted curve shows the experimental relative population of state *F*=3 versus total Raman laser intensity (the ratio of the two lasers is R1/R2=1:5.3). The solid curve shows the fitting.

At this stage, we can define the pulse width (π or $\pi/2$) experimentally. We then changed the optical phase of the final $\pi/2$ pulse gradually by adjusting the voltage applied to the EOM while recording the fluoresce intensity which is proportional to population of the *F*=3 state. A typical interference fringe is shown in Fig. 10, the dots show the experimental data, and the solid line is the fitting. The half-wave voltage of the EOM is 125 V. There are two complete oscillation cycles from 0 to 500V. The relative maximum population is 11, and the minimum population is 5, which gives the fringe contrast of 37% [39].
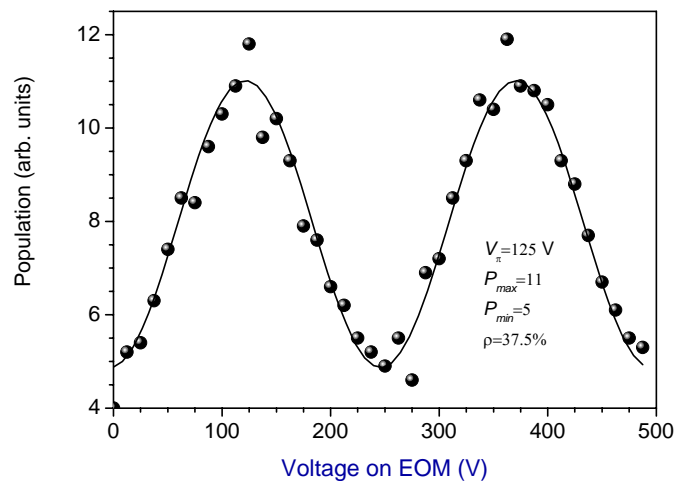

Fig. 10 Interference fringe as a function of relative population to the voltage applied to the EOM. The half-wave voltage of the EOM is 125 V.

We also demonstrated a Ramsey type atom interferometer using two π/2 pulses. The free evolving time between the two pulses was set to be 5.7ms, and the difference frequency of 3GHz to drive the Rabi oscillation was scanned from 3.035,729,200GHz to 3.035,735,200GHz. Fig.11 shows the Ramsey fringe according to the formula

$$P = [1 + cos(\delta T)]/2 \qquad (11)$$

where δ is the detuning of the resonant frequency. The full width at half maximum   FWHM   of the fringe is about 88Hz, and all the data was averaged 4 times.
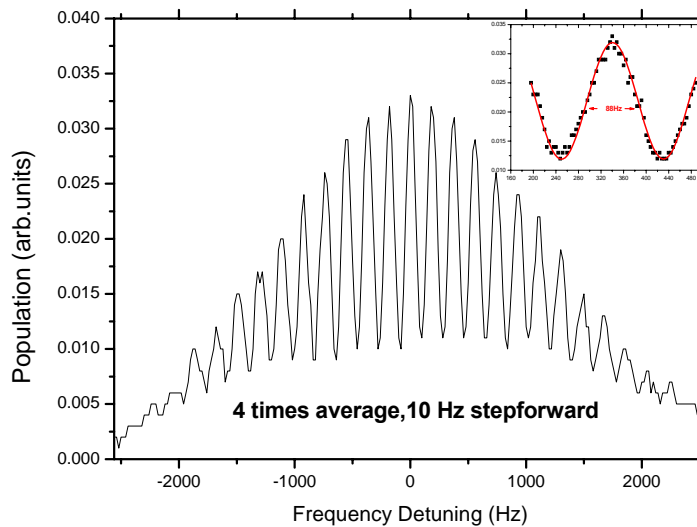

Fig. 11 Ramsey fringe depending on frequency detuning.

In conclusion, we have developed a compact transverse cold [85]Rb atom interferometer. A 1.5 GHz AOM was adopted to produce a pair of Raman lasers, and an EOM was used to change the optical phase of a π/2 pulse. We have successfully realized the cold atom preparation, pushing, optical pumping, Raman population transfer, and finally observed high contrast interference fringe. Following this development of the cold atom Sagnac-type interferometer, the measurement of rotation (atom gyroscope) is underway.

4. Bichromatic Electromagnetically Induced Transparency
Electromagnetically induced transparency (EIT) [40-44] is a quantum interference effect which has been widely studied. In a three-level lambda atomic medium, two lower states are coupled to one excited state by a coupling laser field and a probe laser field. The resonant probe laser beam can pass through the atomic medium without attenuation due to the quantum interference between the dressed states created by the coupling laser beam. It has been shown that EIT has applications in slow light propagation [45-47], coherent nonlinear optics at low light levels [48-51] and quantum information processing [52-55].
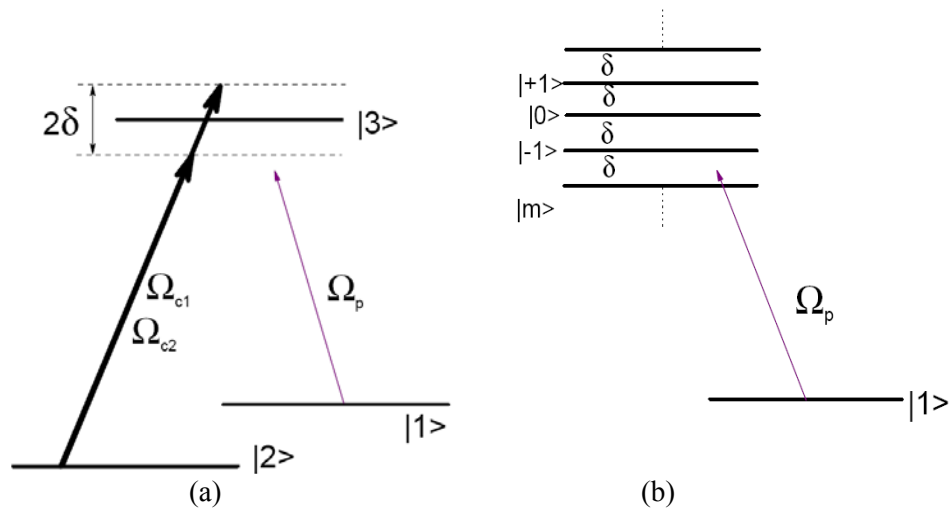
Fig. 12 (a) Three-level Λ type system coupled by a bichromatic field and a weak probe field. (b) Dressed state picture of the coupled three-level system under the symmetrical coupling condition of $(\omega_{c1}+\omega_{c2})/2 = \omega_{23}$.

In the three-level lambda configuration, when the coupling field is a bichromatic field there will appear a series of transparent windows for the weak probe field at multiple frequencies, which is called bichromatic electromagnetically induced transparency and has been experimental demonstrated by us [56]. In Fig. 12 (a), the ground state |2> and the excited state |3> are coupled by two equal-amplitude laser fields Ω_{c1} and Ω_{c2} with a frequency separation 2δ, a weak laser field Ω_p probes the |1>-|3>transition. The dressed states are the superposition of the atomic states |2> and |3> created by the bichromatic field, as shown in Fig. 12 (b), which consist of an infinite ladder with an equal-spacing separation δ between the neighboring levels when the average frequency of the bichromatic field matches the |2>-|3> transition frequency. Such dressed states and the fluorescence spectrum of the two-level atoms coupled by a bichromatic field have been extensively studied before [57-60]. It is expected that the probe absorption spectrum will exhibit multiple peaks corresponding to the dressed transitions |1>-|m> and transparent windows with minimum absorption located near the middle separation of the dressed states. The probe dispersion exhibits a series of normal steep slopes at the absorption minimum, which leads to simultaneous slow group velocities for probe pulses at multiple frequencies separated by δ.

Here we present our new experimental results of bichromatic electromagnetically induced transparency in cold ^{85}Rb atoms. The ^{85}Rb energy-level structure and laser coupling scheme are shown in Fig. 13 (a). A bichromatic coupling laser with frequency separation 40MHz drives the D1 $5S_{1/2}$, F=2-$5P_{1/2}$, F'=3 transition, and a probe laser drives the transition D1 $5S_{1/2}$, F=3-$5P_{1/2}$, F'=3. The trapping laser frequency was red-detuned by an amount ~-15MHz relative to the resonant frequency of the D2 $5S_{1/2}$, F=3-$5P_{3/2}$, F'=4 transition and the repumping laser frequency was locked to the D2 $5S_{1/2}$, F=2-$5P_{3/2}$, F'=3 transition. The trapping, repumping and probe lasers were tuned on and off by three separate acousto-optic modulators (AOMs). For every period of 200ms, the trapping and cooling time was about 198ms (the trapping and repumping lasers were on and the probe laser was off), and the ~2ms was used for data-collection (the trapping and repumping lasers were off and the probe laser was on). The bichromatic coupling field was always on. In this coupling system, during the trapping and cooling time, the bichromatic coupling field can function as another repumping field.
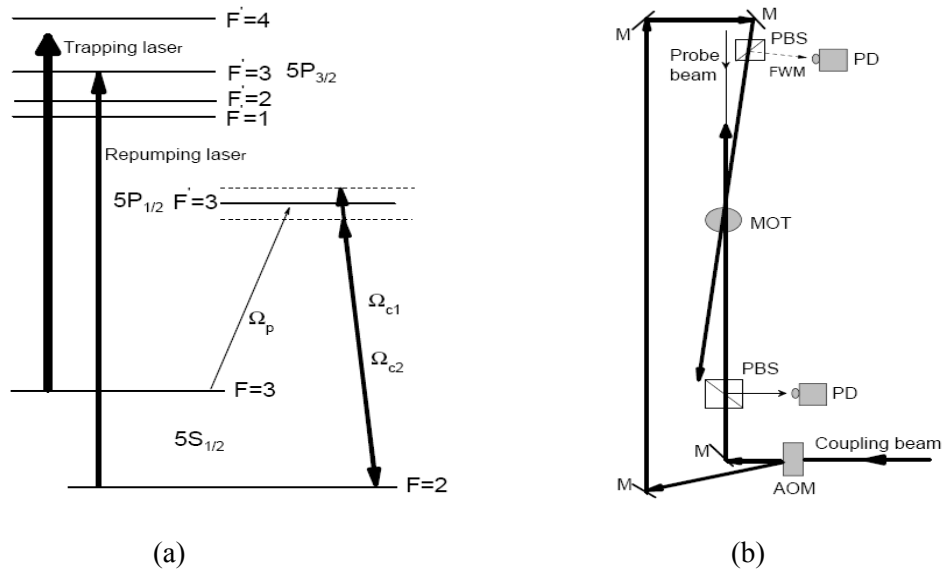
<div style="text-align:center">(a)   (b)</div>

Fig. 13 (a) Energy-level structure of ^{85}Rb and laser coupling scheme. (b) Schematic diagram of the experimental setup. M, mirror; PBS, polarizing beam splitter; PD, photodiode; AOM, acousto-optic modulator.

The schematic diagram of the experimental setup is shown in Fig. 13 (b). The bichromatic coupling field was composed of the diffracted zeroth-order and the first-order beams from a single laser beam passing through a 40MHz AOM. The two coupling beams counter-propagated through the MOT with an angle about ~1^0 and with the same linear polarization. The probe laser beam was linearly polarized perpendicular to the coupling lasers and counter-propagating along the path of one coupling laser beam. Fig. 14 (a) shows the probe transmission spectrum with the coupling Rabi frequency $\Omega_{c1}=\Omega_{c2}=3\Gamma$ ($\Gamma=6$MHz is the natural linewidth of the ^{85}Rb D1 line) and under the symmetrical coupling condition of $(\omega_{c1}+\omega_{c2})/2 = \omega_{23}$. The symmetrical absorption spectrum in Fig. 14 (a) exhibits five absorption peaks with the neighboring peak separation equal to 20MHz, the half frequency difference of the bichromatic coupling field. Increasing the coupling Rabi frequency to $\Omega_{c1}=\Omega_{c2}=4.5\Gamma$, more absorption peaks appear as shown in Fig. 14 (b). These measured probe spectra agree well with the dressed states explanation.

In our experiments, we also observed four-wave mixing (FWM) signal as shown in Fig. 15 (b). The FWM comes from the phase-matched interaction of the two coupling lasers and the probe laser. The phase matching condition is $\vec{k}_p - \vec{k}_{c1} + \vec{k}_{c2} - \vec{k}_{FWM} = 0$ or $\vec{k}_p - \vec{k}_{c2} + \vec{k}_{c1} - \vec{k}_{FWM} = 0$. With the counter-propagation of one coupling laser beam and the probe laser beam, the FWM signal must be in the backward direction of the other coupling laser beam. It's the backward-wave scheme as discussed in Ref.[51], which reported four-wave mixing using EIT in four-level system of cold atoms. We have experimentally demonstrated the backward FWM in three-level system of cold atoms by bichromatic EIT. The detail of this work will be published in other journal.
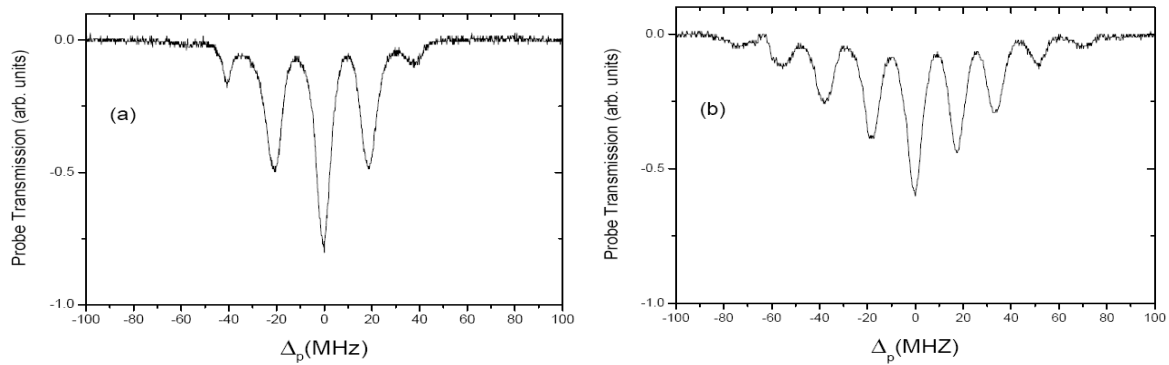
Fig. 14 Measured probe transmission versus the probe detuning under the symmetrical coupling condition of $(\omega_{c1}+\omega_{c2})/2 = \omega_{23}$. (a) $\Omega_{c1}=\Omega_{c2}=3\Gamma$; (b) $\Omega_{c1}=\Omega_{c2}=4.5\Gamma$.
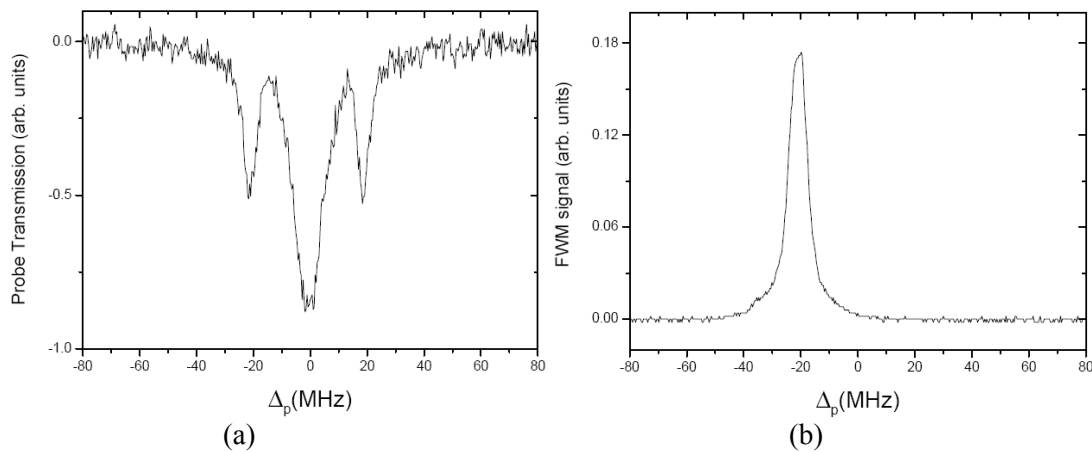

Fig. 15 Measured probe transmission (a) and FWM signal (b) versus the probe detuning under the symmetrical coupling condition of $(\omega_{c1}+\omega_{c2})/2 = \omega_{23}$ and with the coupling intensity $\Omega_{c1}=\Omega_{c2}=2\Gamma$.

References

[1]   Huang K 1987 *Statistical Mechanics*, 2nd Edition (Wiley, New York)
[2]   Bose S N 1924 *Z. Phys.* **26** 178
[3]   Einstein A 1924 *Physikalisch-mathematische Klasse* **1924** 261
[4]   Anderson M H et al 1995 *Science* **269** 198
[5]   Davis K B et al 1995 *Phys. Rev. Lett.* **75** 3969
[6]   Bradley C C et al 1997 *Phys. Rev. Lett.* **78** 985
[7]   Ensher J R et al 1996 *Phys. Rev. Lett.* **77** 4984
[8]   Miesner H J et al 1998 *Science* **279** 13
[9]   Hagley E W et al 1999 *Phys. Rev. Lett.* **83** 3112
[10]   Jin D S et al 1996 *Phys. Rev. Lett.* **77** 420

[11] Abo-Shaeer J R et al 2001 *Science* **292** 476
[12] Esslinger T, Bloch I and Hänsch T W 1998 *Phys. Rev. A* **58** R2664
[13] Lu B L and Wijngaarden W A 2004 *Can. J. Phys.* **82** 81
[14] Raab E et al 1987 *Phys. Rev. Lett.* **59** 2631
[15] Wang J et al 2000 *Acta Optica Sinica 20* 862
[16] Jiang K J et al 2003 *Chin. Opt. Lett.* **1** 377
[17] Monroe C et al 1990 *Phys. Rev. Lett.* **65** 1571
[18] Dalibard J and Cohen-Tannoudji C 1989 *J. Opt. Soc. Am. B* **6** 2023
[19] Arnold A 1999 *Ph.D. thesis* (University of Sussex)
[20] Xiong H W et al 2003 *J. Phys. B* **36** 3315
[21] Xiong H W, Liu S J and Zhan M S 2006 *New J. Phys.* **8** 245
[22] Berman P R (ed.) 1997 *Atom Interferometry* (Academic Press, San Diego)
[23] Arlt J et al 2005 *Adv. At. Mol. Opt. Phys.* **50** 55
[24] Zhou S K and Zhan M S 1993 *Chinese J. Quantum Electronics* **10** 91
[25] Lenef A et al 1997 *Phys. Rev. Lett.* **78** 760
[26] Gustavson T L et al 1997 *Phys. Rev. Lett.* **78** 2046
[27] McGuirk J M et al 2002 *Phys. Rev. A* **65** 033608
[28] Peters A et al 2001 *Metrologia* **38** 25
[29] Snadden M J et al 1998 *Phys. Rev. Lett.* **81** 971
[30] Peters A et al 1999 *Nature* **400** 849
[31] Weiss D S et al 1993 *Phys. Rev. Lett.* **70** 2706
[32] Wicht A et al 2002 *Physica Scripta* **T102** 82
[33] Torii Y et al 2000 *Phys. Rev. A* **61** 041602
[34] Canuel B et al 2006 *Phys.Rev.Lett.* **97** 010402
[35] Jiang K J et al 2005 *Chin. Phys. Lett.* **22** 324
[36] Kasevich M and Chu S 1992 *Appl. Phys. B* **54** 321
[37] Kasevich M et al 1991 *Phys. Rev. Lett.* **66** 2297
[38] Moler K et al 1992 *Phys.Rev. A* **45** 342
[39] Wang P et al 2007 *Chin. Phys. Lett.* **24** 27
[40] Harris S E 1997 *Phys. Today* **50** 36
[41] Marangos J P 1998 *J. Mod. Opt.* **45** 471
[42] Boyd R W and Gauthier D J 2002 *Progress in Optics* **43** 497
[43] Fleischhauer M et al 2005 *Rev. Mod. Phys.* **77** 633
[44] Wang J et al 2004 *Phys. Lett. A* **328** 437
[45] Hau L V et al 1999 *Nature* **397** 594
[46] Kash M M et al 1999 *Phys. Rev. Lett.* **82** 5229
[47] Tu X H et al 2003 *Chin. Phys. Lett.* **20** 1954
[48] Harris S E, Field J E and Imamoglu A 1990 *Phys. Rev. Lett.* **64** 1107
[49] Schmidt H and Imamoglu A 1996 *Opt. Lett.* **21** 1936; Kang H and Zhu Y F 2003 *ibid.* **91** 093601
[50] Kong L B et al 2005 *Opt. Commun.* **255** 331
[51] Braje D A et al 2004 2004 *Phys. Rev. Lett.* **93** 183601
[52] Liu C et al 2001 *Nature* **409** 490
[53] Chaneliere T et al 2005 *Nature* **438** 833
[54] Eisaman M D et al 2005 *Nature* **438** 837
[55] Jing H et al 2005 *Phys. Rev. A* **71** 062336
[56] Wang J et al 2003 *Phys. Rev. A* **68** 063810
[57] Zhu Y F et al 1990 *Phys. Rev. A* **41** 6574
[58] Freedhoff H and Chen Z 1990 *Phys. Rev. A* **41** 6013
[59] Agarwal G S et al 1991 *J. Opt. Soc. Am. B* **8** 1163
[60] Ficek Z and Freedhoff H S 1993 *Phys. Rev. A* **48** 3092